

Journal of Materials Chemistry C

Accepted Manuscript



This is an *Accepted Manuscript*, which has been through the Royal Society of Chemistry peer review process and has been accepted for publication.

Accepted Manuscripts are published online shortly after acceptance, before technical editing, formatting and proof reading. Using this free service, authors can make their results available to the community, in citable form, before we publish the edited article. We will replace this *Accepted Manuscript* with the edited and formatted *Advance Article* as soon as it is available.

You can find more information about *Accepted Manuscripts* in the [Information for Authors](#).

Please note that technical editing may introduce minor changes to the text and/or graphics, which may alter content. The journal's standard [Terms & Conditions](#) and the [Ethical guidelines](#) still apply. In no event shall the Royal Society of Chemistry be held responsible for any errors or omissions in this *Accepted Manuscript* or any consequences arising from the use of any information it contains.

COMMUNICATION

Direct Growth of Graphene Nanopatches on Graphene Sheets for Highly Conductive Thin Film Applications[†]

Cite this: DOI: 10.1039/x0xx00000x

Wooseok Song,^{a,c} Ki Woong Kim,^{a,c} Sung-Jin Chang,^b Tae Jung Park,^b Sung Ho Kim,^a Min Wook Jung,^a Geonhee Lee,^a Sung Myung,^{a,*} Jongsun Lim,^a Sun Suk Lee,^a and Ki-Seok An^aReceived 00th January 2012,
Accepted 00th January 2012

DOI: 10.1039/x0xx00000x

www.rsc.org/

Graphene nanopatches (GNs) on graphene films grown by chemical vapor deposition (CVD) were synthesized by Ni nanoparticle assembly and subsequent CVD growth to enhance their electrical conductivity. As a result, the sheet resistance of hexagonally shaped GN-assembled graphene films decreased from 681.7 ± 11.2 to 527.2 ± 47.0 Ω/sq with 97.9% transparency. This improvement in electrical conductivity was a result of p-type doping of the GNs on graphene films and the generation of additional charge carrier conducting paths to diminish defect scattering, which was a result of enhanced extracted-hole mobility of the GN-assembled graphene films.

Recently, direct synthesis of graphene using a chemical vapor deposition (CVD) process has been considered a facile approach to producing large-area uniform graphene films to replace indium tin oxide (ITO) in transparent and flexible electronics.¹⁻⁶ However, the structure and quality of CVD-graphene films are very sensitive to preparation conditions such as humidity, temperature and gas flow, and CVD graphene has a polycrystalline structure prone to topological defects such as dislocations and grain boundaries. These defects can scatter the charge carrier, resulting in significant deterioration in the electrical conductivity of graphene films.^{7,8} Therefore, many efforts are being devoted to the synthesis of high-quality graphene sheets via the healing processes of defect-rich graphene layers. This process enhances electrical conductivity by employing various nanostructures as dopants to control the carrier concentration in graphene.⁹⁻¹¹ For instance, metal nanowires (NWs) and carbon nanotubes (CNTs) have been assembled with CVD-graphene films in order to decrease the sheet resistance by allowing the metal NWs and CNTs to bridge structural defects and avoid disruption in the graphene films.^{12,13} However, the high contact resistance between NWs/CNTs and the graphene films and a significant loss of optical transmittance in hybrid graphene films remain obstacles to achieving high-performance transparent electrodes (TEs).

In this communication, we suggested a facile methodology to enhance the electrical conductivity in CVD-graphene films by assembly of Ni nanoparticles (NPs) and subsequent growth of graphene nanopatches (GNs) on graphene films. The optical transmittance and sheet resistance of the GNs were examined in order to ascertain the capabilities of graphene-based TEs. This assembly process achieved enhancement of the electrical conductivity with a negligible loss of optical transmittance in the GNs on graphene films. We also demonstrated the potential for GN-assembled graphene sheets as TEs in a transparent prototype capacitor for an electrostatic touch panel. This approach will provide an efficient synthesis method for high-quality graphene sheets by reusing low-quality graphene films grown under non-optimized growth conditions, and will reduce the production cost of high-quality graphene sheets.

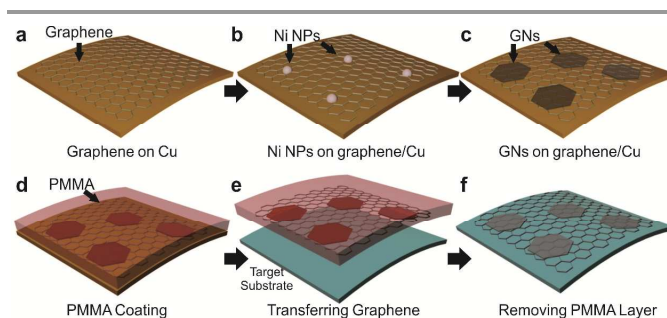


Fig. 1. Schematic diagrams of the formation of GNs on graphene/Cu via Ni NP assembly on graphene films and subsequent CVD growth.

Fig. 1a shows schematic diagrams of the formation of GNs on graphene films synthesized on Cu for improved electrical conductivity of graphene-based TEs. First, a single layer graphene on Cu foil was synthesized via thermal CVD. The Cu foil was heated to 1000 °C in the CVD chamber, and graphene was synthesized sequentially on the Cu surface by introducing

CH₄ gas with H₂ and Ar. This large-scale CVD-grown graphene sheet had a poly-crystalline structure and the nature of the domain boundaries. These structural defects may act as internal scattering centers for electron waves and degrade the transport properties of graphene compared to the theoretical value or data from exfoliated graphene.^{14,15} Solving the problem of the suboptimal electrical property required either the integration of graphene and nanostructures to increase graphene conductance or the healing of low-quality graphene sheets without the degradation of the optical transmittance and electrical conductance. Here, we synthesized GNs on CVD-graphene using Ni NPs as catalysts, and utilized GNs as electrical bridges between CVD-graphene grain boundaries or through structural defects. Ni NPs for GN synthesis were assembled on graphene films by dipping them in NiCl₂ solution (Fig. 1b). Most Ni NPs were located on defects or disruptions such as wrinkles, ripples, and folds due to the oxygen-rich functional groups and the high reactivity of the defects and disruptions. The formation of disruptions originated from the difference between the thermal expansion coefficient of the Cu and that of the graphene film.¹⁶ After the second CVD growth of GNs on the graphene sheets, the CVD reactor was cooled to room temperature (Fig. 1c). Poly(methylmethacrylate) (PMMA) was spin-coated onto the graphene sheet with GNs, and the Cu foil was removed by copper etchant (dilute FeCl₃ solution in deionized water). The PMMA-coated graphene sheet was then transferred to a target substrate, such as SiO₂ or polyethylene terephthalate (PET). Finally, PMMA was carefully removed by acetone (Fig. 1d-f). Importantly, in our conductance-enhancing process, GNs were synthesized directly on the graphene sheet. Because graphene with GNs was stable during PMMA-assisted wet-transferring, it was more suitable for the graphene-based devices or TEs than graphene composites such as graphene sheets attached with metal NWs.

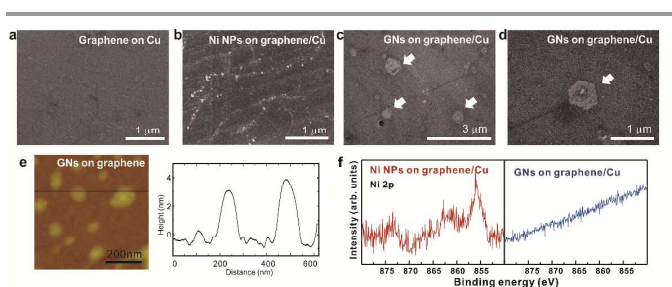


Fig. 2. Characterization of graphene nanosheets with GNs. SEM images of (a) pristine graphene on Cu, (b) Ni NPs distributed on graphene/Cu foil, and (c,d) GNs on graphene/Cu after the second CVD growth. (e) AFM images of GNs on graphene/Cu foil after the second CVD growth and the height profile. (f) Ni 2p XPS spectra of Ni NP-assembled graphene and graphene sheets with GNs.

The presence of wrinkles was observed in pristine CVD-graphene on Cu foil, as shown in Fig. 2a. After the assembly of Ni NPs in the NiCl₂ solution, well-defined spherical NPs were formed adjacent to the defects or wrinkles in the graphene sheets (Fig. 2b). This result can be explained by the fact that the defects or curvature induced by the wrinkles created stable nucleation centers for nano-particulation. The formation of wrinkles originated from the difference between the thermal expansion coefficient of the Cu and that of the graphene film.¹⁶ After the second CVD growth, hexagonally-shaped GNs adjacent to the defects or wrinkles were formed unambiguously (Fig. 2c,d). GNs with specific crystallographic direction were

synthesized on the Ni NPs formed at the defects or wrinkles. The formation of GNs on graphene films implied that Ni NPs played a crucial role in the formation of nucleation sites for GNs. Additionally, similar to a previous report, the shape and size of the graphene domain could also be controlled by adjusting growth conditions.⁸ Fig. 2e exhibits atomic force microscope (AFM) images of GNs on graphene films, showing a GN height of approximately 3-4 nm. The Ni 2p X-ray photoelectron spectroscopy (XPS) of graphene sheets after Ni NP assembly and the second CVD process is shown in Fig. 2f. The spectrum can roughly be divided into two peaks split by spin-orbit coupling, corresponding to 2p_{1/2} (E_B = 873.8 eV) and 2p_{3/2} (E_B = 855.9 eV) of NiCl₂. After the formation of the GNs, the Ni 2p peaks disappeared, presumably due to either the presence of 3-nm-thick GNs or the thermal evaporation of Ni NPs.

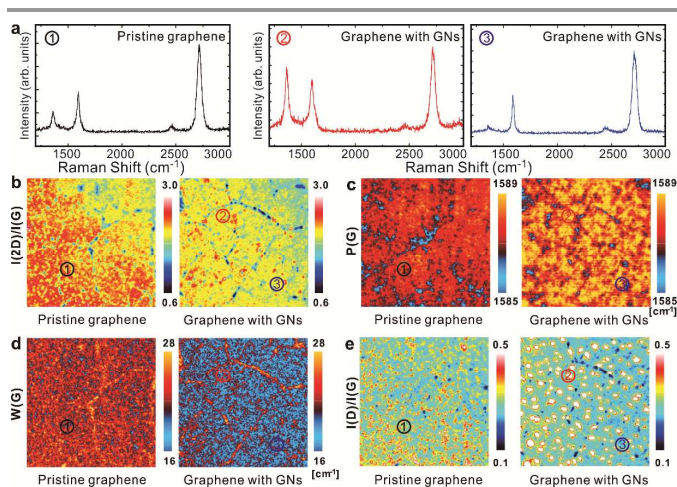


Fig. 3. Spectroscopic Raman mapping of graphene-based sheets. (a) Raman spectra for pristine graphene, graphene sheets with GNs after the second CVD growth (b) I_{2D}/I_G map, (c) G-band position map, (d) G-band FWHM map, and (e) I_D/I_G map for pristine graphene and GNs on graphene.

The electrical interaction between the graphene film and the GNs was analyzed by resonant Raman spectroscopy. The Raman spectra of pristine graphene, non-Ni-treated and GN-assembled, clearly showed the graphene fingerprints, the D-, G-, and 2D-bands (Fig. 3a). The G-band is associated with normal first-order Raman scattering involving an electron and doubly degenerated phonons (iTO and iLO) at the zone center.¹⁷ The 2D-band originated from an intervalley, double-resonance Raman process which involved an electron and two iTO phonons at the K point.¹⁷ Raman maps taken from each graphene film transferred onto SiO₂ substrates showed discernible variations in the intensity ratio of 2D- to G-bands (I_{2D}/I_G), the position of the G-band (P(G)), the full-width at half maximum (FWHM) of the G-band (W(G)), and the intensity ratio of D- to G-bands (I_D/I_G) (Fig. 3b-e). Of particular interest was the significant decrease in the I_{2D}/I_G value of GN-assembled graphene sheets compared with pristine graphene. The G-band experienced a blueshift and the FWHM of the G-band decreased, which indicated p-type doping by charge transfer from the GNs to graphene. This process was induced by the work function difference between the materials due to the existence of oxygen-containing functional groups (-OH and -COOH) at the edge of the GNs, which were supported by the Raman map of I_D/I_G (Fig. 3e). One important criterion in the

synthesis method for industrial applications is the uniformity of GN-assembled graphene sheets, and this Raman analysis of large-scale graphene sheets with GNs ($40\ \mu\text{m} \times 40\ \mu\text{m}$) confirmed that GNs were synthesized uniformly on single graphene sheets. These results proved that our method could be applied to convert low-quality graphene sheets into graphene for industrial-level TEs.

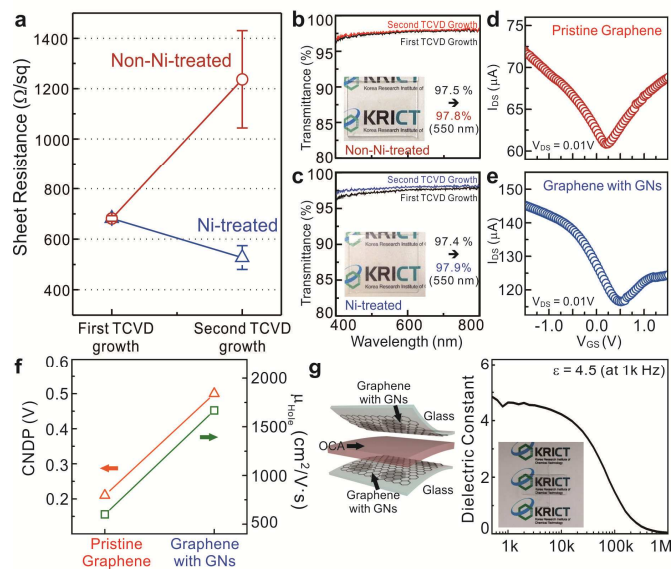


Fig. 4. (a) Sheet resistance and (b, c) optical transmittance of non-Ni-treated and Ni-treated graphene sheets as a function of CVD cycle. Photographs of non-Ni-treated graphene (inset in (b)) and Ni-treated graphene (inset in (c)) onto glass substrates after the second CVD growth. Transfer curves ($V_{\text{DS}} = 0.01$ V) of (d) pristine graphene and (e) graphene films with GNs at room temperature. (f) Plots of the CNDP and the μ_{hole} for pristine graphene and the GNs on graphene. (g) Schematic illustration (left) and frequency dependency of the dielectric constant (right) of the capacitor based on graphene sheets with GNs.

Fig. 4a illustrates the sheet resistance of non-Ni-treated and Ni-treated graphene films transferred onto SiO_2 (300 nm)/ $\text{Si}(001)$ substrates as a function of CVD cycle. First, a graphene layer with a sheet resistance of 681.7 ± 11.2 Ω/sq was prepared. After the second CVD process, the sheet resistance of the non-Ni-treated graphene sheet increased significantly (1237 ± 193.2 Ω/sq). This result suggested that structural defects were inevitably formed on graphene sheets when H_2 gas was introduced at high temperature during the second CVD process, resulting in an increase in electrical resistance. Conversely, the sheet resistance of Ni-treated graphene formed by assembling Ni NPs on graphene in NiCl_2 solution decreased from 681.7 ± 11.2 to 527.2 ± 47.0 Ω/sq after the second CVD process. In a previous report, CVD-graphene assembled with metal MWs dramatically decreased the resistance of graphene films.¹² Similarly, the GNs synthesized in this study bridged structural defects and repaired disruptions in graphene films, which dramatically reduced the sheet resistance of graphene. Although the GNs were formed on graphene films, the optical transmittance at 550 nm of the films increased slightly. This result could be explained by the removal of amorphous carbon on the graphene films during the second CVD process (Fig. 4c). This result indicated that the conditions employed for the formation of the GN optimized its size and density, and

enhancement of the electrical conductivity was achieved with a negligible variation of optical transmittance in graphene-based TEs by inducing the formation of the GNs on graphene films. In order to evaluate the electrical transport properties of GNs on graphene films, we fabricated electrochemically gated graphene-based field effect transistors (FETs).^{18,19} Fig. 4d,e shows transfer curves ($I_{\text{DS}}-V_{\text{GS}}$) of graphene-based FETs and GN-assembled graphene FETs. The transfer curve at $V_{\text{DS}} = 0.01$ V exhibited ambipolar behavior with a charge neutral Dirac point (CNDP) at 0.21 V and hole-electron conduction asymmetry due to the unintentional p-type doping of the graphene by water molecules.²⁰ In the case of the GN-assembled graphene FETs, a significant shift in the CNDP toward a positive V_{GS} at 0.5 V was observed unambiguously, indicating p-type doping of the GNs on graphene films. Based on the transfer curves, the extracted hole mobility (μ_{hole}) was 601 $\text{cm}^2/\text{V}\cdot\text{s}$ for the graphene FETs and 1668 $\text{cm}^2/\text{V}\cdot\text{s}$ for the GNs (Fig. 4f). This result may have been due to the additional conducting paths for the charge carrier in graphene generated during formation of the GN-assembled graphene sheets generated, which diminished the defect scattering. These GN-assembled graphene sheets were tested as a TE in a graphene-based metal-insulator-metal (MIM) capacitor, which has been integrated into mutual-capacitive touch screens. In our experiment, two TEs were replaced by graphene sheets with GNs on glass substrates (Fig. 4g). A commercial flexible optical clean adhesive (OCA, 3M, 100- μm -thick) film was utilized as the organic insulator between the two graphene-based TEs. The dependence of the dielectric constant (ϵ) of graphene-based capacitors as a function of frequency is shown in Fig. 4g. The dielectric constant was 4.5 at 1 kHz as the applied frequency was increased from 1 kHz to 1 MHz, which was similar to the CVD graphene-based capacitor and Au/OCA/ITO capacitor in our previous studies.²¹ This analysis showed that a graphene-based transparent capacitor can be synthesized using only graphene sheets converted from low quality graphene films. This method may pave the way for industrial-level production of graphene-based TEs.

Conclusions

We demonstrated a facile method to improve electrical conductivity via the formation of GNs on CVD-graphene sheets. After Ni NP assembly and subsequent CVD growth, hexagonally-shaped GNs were observed adjacent to the wrinkles and defects in graphene films. The sheet resistance of graphene films decreased from 681.7 ± 11.2 to 527.2 ± 47.0 Ω/sq with 97.9% transparency after the formation of the GNs. Raman spectroscopy and electrical transport measurements suggested that this improved electrical conductivity was a result of p-type doping of the GNs. This effect was most likely due to charge transfer from the GNs to graphene, which originated from the higher work function of the GNs due to the oxygen-containing functional groups ($-\text{OH}$ and $-\text{COOH}$) at the edge of the GNs. In addition, the extracted hole mobility of the GN-assembled graphene films increased significantly from 601 to 1668 $\text{cm}^2/\text{V}\cdot\text{s}$. Notably, these results may present a feasible and reliable route for enhancing electrical conductivity in graphene-based TEs with a negligible loss of optical transmittance.

Acknowledgements

This research was supported by a grant (2011-0031636) from the Center for Advanced Soft Electronics under the Global Frontier Research Program of the Ministry of Science, ICT and Future Planning, Korea and by a grant from the Technology Development Program for Strategic Core Materials funded by the Ministry of Trade, Industry & Energy, Republic of Korea (Project No. 10047758).

Author contributions

K.W.K, S.H.K and M.W.J prepared and characterize CVD-grown graphene sheets: K.W.K performed Ni NP assembly and second CVD process for graphene nanopatches; G.L provided AFM images of graphene sheets with nanopatches: J.L. and K.A. performed XPS and electrical experiments and contributed to interpretation of the results: S.J and T.P. contributed to Raman mapping and interpretation of Raman results: S.M. conceived and designed the experiments: W.S and S.M wrote the main paper and K.W.K and S.S.L. prepared supporting information; All authors discussed the results and implications and commented on the manuscript.

Notes and references

^a *Thin Film Materials Research Group, Korea Research Institute of Chemical Technology (KRICT), Yuseong Post Office Box 107, Daejeon 305-600, Republic of Korea E-mail: msung@kRICT.re.kr*

^b *Department of Chemistry, Chung-Ang University, 84 Heukseok-ro, Dongjak-gu, Seoul, 156-756, Republic of Korea*

^c *These authors contributed equally to this work.*

[†] *Electronic Supplementary Information (ESI) available: Experimental details, preparation and measurement of electronic devices based on graphene with GNs. See DOI: 10.1039/c000000x/*

- 1 K. S. Novoselov, A. K. Geim, S. V. Morozov, D. Jiang, Y. Zhang, S. V. Dubonos, I. V. Grigorieva and A. A. Firsov, *Science*, 2004, **306**, 666.
- 2 K. S. Novoselov, Z. Jiang, Y. Zhang, S. V. Morozov, H. L. Stormer, U. Zeitler, J. C. Maan, G. S. Boebinger, P. Kim and A. K. Geim, *Science*, 2007, **315**, 1379.
- 3 R. R. Nair, P. Blake, A. N. Grigorenko, K. S. Novoselov, T. J. Booth, T. Stauber, N. M. R. Peres, and A. K. Geim, *Science*, 2008, **320**, 1308.
- 4 K. S. Kim, Y. Zhao, H. Jang, S. Y. Lee, J. M. Kim, K. S. Kim, J. -H. An, P. Kim, J. -Y. Choi and B. H. Hong, *Nature*, 2009, **457**, 706.
- 5 X. Li, W. Cai, J. An, S. Kim, J. Nah, D. Yang, R. Piner, A. Velamakanni, I. Jung, E. Tutuc, S. K. Banerjee, L. Colombo and R. S. Ruoff, *Science*, 2009, **324**, 1312.
- 6 S. Bae, H. Kim, Y. Lee, X. Xu, J. -S. Park, Y. Zhang, J. Balakrishnan, T. Lei, H. R. Kim, Y. I. Song, Y. -J. Kim, K. S. Kim, B. Ozyilmaz, J. -H. Ahn, B. H. Hong and S. Iijima, *Nat. Nanotechnol.*, 2010, **5**, 574.
- 7 O. V. Yazyev and S. G. Louie, *Nat. Mater.*, 2010, **9**, 806.
- 8 Q. Yu, L. A. Jauregui, W. Wu, R. Colby, J. Tian, Z. Su, H. Cao, Z. Liu, D. Pandey, D. Wei, T. F. Chung, P. Peng, N. P. Guisinger, E. A. Stach, J. Bao, S. -S. Pei and Y. P. Chen, *Nat. Mater.*, 2011, **10**, 443.
- 9 K. K. Kim, A. Reina, Y. Shi, H. Park, L. -J. Li, Y. H. Lee and J. Kong, *Nanotechnology*, 2010, **21**, 285205.

- 10 K. C. Kwon, K. S. Choi and S. Y. Kim, *Adv. Funct. Mater.*, 2012, **22**, 4724.
- 11 Y. Kim, W. Song, S. -I. Lee, S. Y. Lee, M. -J. Cha, D. S. Jung and C. -Y. Park, *Appl. Phys. Lett.*, 2013, **102**, 223116.
- 12 I. N. Kholmanov, C. W. Magnuson, A. E. Aliev, H. Li, B. Zhang, J. W. Suk, L. L. Zhang, E. Peng, S. H. Mousavi, A. B. Khanikaev, R. Piner, G. Shvets and R. S. Ruoff, *Nano Lett.*, 2012, **12**, 5679-5683.
- 13 S. H. Kim, W. Song, M. W. Jung, M. -A. Kang, K. Kim, S. -J. Chang, S. S. Lee, J. Lim, J. Hwang, S. Myung and K. -S. An, *Adv. Mater.*, 2014, **26**, 4247.
- 14 N. Petrone, C. R. Dean, I. Meric, A. M. van der Zande, P. Y. Huang, L. Wang, D. Muller, K. L. Shepard and J. Hone, *Nano Lett.*, 2012, **12**, 2751-2756.
- 15 A. W. Tsen, L. Brown, M. P. Levendorf, F. Ghahari, P. Y. Huang, R. W. Havener, C. S. Ruiz-Vargas, D. A. Muller, P. Kim and J. Park, *Science*, 2012, **336**, 1143-1146.
- 16 S. J. Chae, F. Gunes, K. K. Kim, E. S. Kim, G. H. Han, S. M. Kim, H. -J. Shin, S. -M. Yoon, J. -Y. Choi, M. H. Park, C. W. Yang, D. Pribat and Y. H. Lee, *Adv. Mater.*, 2009, **21**, 2328.
- 17 L. M. Malard, M. A. Pimenta, G. Dresselhaus and M. S. Dresselhaus, *Phys. Rep.*, 2009, **473**, 51.
- 18 F. Chen, Q. Qing, J. Xia, J. Li and N. Tao, *J. Am. Chem. Soc.*, 2009, **131**, 9908.
- 19 W. Song, S. Y. Kim, Y. Kim, S. H. Kim, S. I. Lee, I. Song, C. Jeon and C. -Y. Park, *J. Phys. Chem. C*, 2012, 116, 20023.
- 20 W. Zhang, C. -T. Lin, K. -K. Liu, T. Tite, C. -Y. Su, C. -H. Chang, Y. -H. Lee, C. -W. Chu, K. -H. Wei, J. -L. Kuo and L. -J. Li, *ACS Nano*, 2011, **5**, 7517.
- 21 H. S. Kim, M. W. Jung, S. Myung, D. S. Jung, S. S. Lee, K. J. Kong, J. S. Lim, J. H. Lee, C. Y. Park and K. S. An, *J. Mater. Chem. C*, 2013, **1**, 1076.